SPHERA
A Unifying Structure from Motion Framework for Central Projection Cameras

Christiano Couto Gava[1,2] and Didier Stricker[1,2]

[1]*Department Augmented Vision, German Research Center for Artificial Intelligence, Kaiserslautern, Germany*

[2]*Department of Informatics, Technical University of Kaiserslautern, Kaiserslautern, Germany*

Keywords: Spherical Images, Structure from Motion, Central Projection Cameras, 3D Reconstruction.

Abstract: As multi-view reconstruction techniques evolve, they accomplish to reconstruct larger environments. This is possible due to the availability of vast image collections of the target scenes. Within the next years it will be necessary to account for all available sources of visual information to supply future 3D reconstruction approaches. Accordingly, Structure from Motion (SfM) algorithms will need to handle such variety of image sources, i.e. perspective, wide-angle or spherical images. Although SfM for perspective and spherical images as well as catadioptric systems have already been studied, state of the art algorithms are not able to deal with these images simultaneously. To close this gap, we developed SPHERA, a unifying SfM framework designed for central projection cameras. It uses a sphere as underlying model, allowing single effective viewpoint vision systems to be treated in a unified way. We validate our framework with quantitative evaluations on synthetic spherical as well as real perspective, spherical and hybrid image datasets. Results show that SPHERA is a powerful framework to support upcoming algorithms and applications on large scale 3D reconstruction.

1 INTRODUCTION

The popularity of full panoramic images has significantly increased during the past few years. This is confirmed by the variety of spherical image acquisition hardware and software packages available nowadays (Civetta, 2009), (LizardQ, 2014), (Seitz-Roundshot, 2014), (PTgui-Pro, 2014). Another reason for the increased popularity of such images is the possibility to create immersive environments where the user experiences a first-person view, such as Google Street View (Anguelov et al., 2010). Full spherical images are specially attractive for this kind of visualization as well as 3D reconstruction of large scenes. These applications find appliance in documentation, education, preservation of cultural heritage, gaming, city planing, etc. Applications based on multi-view reconstruction usually require the acquisition of several images to produce a 3D model of the target scene. Hence, they implicitly demand Structure from Motion (SfM) to recover the cameras' poses before the 3D model can be computed.

Spherical images are also more suitable for SfM than standard perspective images. Due to their wide field of view, scene features are observed in more images, thus increasing the number of constraints on cameras' poses. Consequently, methods have been derived to perform SfM on wide field of view cameras. More specifically, (Chang and Hebert, 2000), (Micusik and Pajdla, 2006), (Bagnato et al., 2011) address SfM on omnidirectional images, while (Kangni and Laganiere, 2007), (Pagani and Stricker, 2011), (Aly and Bouguet, 2012) deal with full spherical images. Not surprisingly, perspective SfM has been extensively studied e.g. by (Snavely et al., 2006), (Hartley and Zisserman, 2004), (Ma et al., 2003). Although these approaches have shown to work well for the specific image type they were designed for, up to the authors knowledge they are unable to handle images of any other type.

Given the current effort to reconstruct ever growing environments (Agarwal et al., 2009), (Furukawa et al., 2010) every source of visual information shall be taken into account, regardless of the shape of image surface. This is an issue that has not yet being addressed. Apart from performance and accuracy, another highly desirable feature of 3D reconstruction algorithms is to update and improve the scene model whenever new images are available. Here again, the ability to deal with different camera types is essential. Therefore, we present SPHERA, a novel Structure from Motion framework to bridge the gap between

Gava C. and Stricker D..
SPHERA - A Unifying Structure from Motion Framework for Central Projection Cameras.
DOI: 10.5220/0005301702850293
In *Proceedings of the 10th International Conference on Computer Vision Theory and Applications* (VISAPP-2015), pages 285-293
ISBN: 978-989-758-091-8

current SfM methods for central projection cameras. We build on the model proposed in (Geyer and Daniilidis, 2001) and adopt the unit sphere to represent images and to treat heterogeneous camera types in an unified way. Our approach dynamically selects the best information available to recover camera poses and scene structure. Experiments on synthetic and real image sequences validate our framework as a valuable contribution to support large scale 3D reconstruction algorithms.

Related Work

The work presented in (Chang and Hebert, 2000) uses epipolar geometry to compute scene structure from an omnidirectional vision system mounted on a robot platform. However, the camera pose problem is not addressed. In (Micusik and Pajdla, 2006), the authors focus on omnidirectional images with a field of view larger than 180^o and devise a camera model specific for that type of image. Although scene structure can be recovered, the technique is limited to the two-view geometry problem. Consequently, the proposed camera model can hardly be used in a more generic SfM approach. In (Bagnato et al., 2011), the authors present a variational approach to achieve egomotion estimation and 3D reconstruction from omnidirectional image sequences. Nonetheless, the environment must be densely sampled so that the relationship between image derivatives and 3D motion parameters is still valid. Thus, this approach can not be used in a more general, sparse SfM.

A method to recover camera poses from a set of spherical images on a sparsely sampled environment is presented in (Kangni and Laganiere, 2007). However, SfM is performed based on panoramic cubes computed for each spherical image. That is, the camera poses are recovered by casting the spherical problem back to the standard perspective problem. In (Aly and Bouguet, 2012), spherical images are used to estimate the relative camera poses and to build a map of the environment. To simplify the problem, Aly and Bouguet assume planar motion, i.e. all camera frames lie on the same plane. This assumption strongly limits the applicability of the proposed technique. Finally, our approach is closely related to (Pagani and Stricker, 2011), as both exploit full spherical images to deliver a sparse representation of the scene along with recovered camera poses. Nevertheless, the method presented in (Pagani and Stricker, 2011) was designed exclusively for spherical cameras, whereas our framework naturally handles any kind of central projection camera.

2 BACKGROUND

2.1 Spherical Images

A spherical image is a $180^o \times 360^o$ environment mapping that allows an entire scene to be captured from a single point in space. Consequently, every visible 3D point P_W given in world coordinate system can be mapped onto the image surface. This is done by a two-step process. First, analogue to the perspective case, P_W is represented in the camera coordinate system as $P_C = RP_W + t$, with R and t representing the camera rotation matrix and translation vector. Second, and different from the perspective projection, P_C is projected onto the image surface by scaling its coordinates, as shown in Fig. 1-(a). Without loss of generality, we assume a unit sphere. Thus, the scaling becomes a normalization and $p = P_C/\|P_C\|$.

Spherical images are stored as a 2D pixel-map as depicted in Fig. 1-(b). This map is obtained using a latitude-longitude transformation, with $0 \leq \phi \leq \pi$ and $0 \leq \theta \leq 2\pi$.

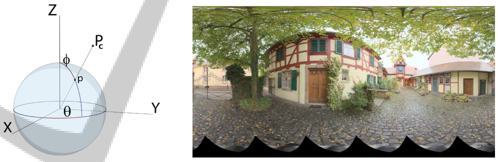

(a) (b)

Figure 1: (a) Spherical coordinates and illustration of the spherical projection. (b) Pixel-map of a spherical image.

2.2 Sphere as Unifying Model

Our approach is grounded on the seminal work developed in (Geyer and Daniilidis, 2001), where the authors proposed a unifying model for the projective geometry of vision systems having a single effective viewpoint. These vision systems are commonly referred to as central projection cameras and include catadioptric sensors featuring conic mirrors of different shapes, such as parabolic, hyperbolic or elliptic. Geyer and Daniilidis showed that any central catadioptric projection is equivalent to a two-step mapping via the sphere. It is well known from the pinhole model that standard perspective imaging characterizes a single viewpoint system. Nonetheless, perspective images are also central catadioptric systems with a virtual planar mirror and are, therefore, covered by the aforementioned model. In practice, that means it is possible to treat these central projection systems as spherical cameras, provided the mapping from the original image surface to the sphere is known. This mapping may be seen as a warping transformation from the original image to the unit sphere. As an example, Fig. 2 shows the result of warping a perspective image onto the sphere.

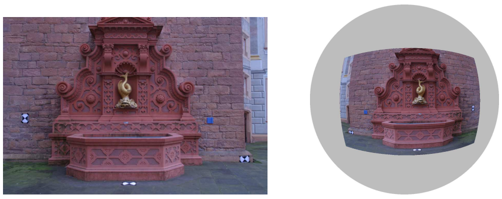
(a) (b)

Figure 2: Example of (a) an original perspective image (Strecha et al., 2008) and (b) its warped version. The warped image appears mirrored due to the viewpoint ("outside" the unit sphere).

2.3 Spherical Camera Pose Estimation

2.3.1 Epipolar Geometry

The epipolar geometry for full spherical cameras has already been presented in (Torii et al., 2005). Thus, here we provide a short overview. Consider a pair of spherical cameras C_0 and C_1. Let R and t be the associated rotation matrix and translation vector. A point p_0 on the surface of C_0, along with the centers of the cameras, define a plane Π that may be expressed by its normal vector $n_\Pi = Rp_0 \times t = [t]_\times Rp_0$, where $[t]_\times$ is the skew-symmetric matrix representing the cross-product. For any point p_1 on C_1 belonging to Π the condition $p_1^T n_\Pi = 0$ holds, which is equivalent to $p_1^T [t]_\times Rp_0 = 0$, where $E = [t]_\times R$ is the essential matrix (Hartley and Zisserman, 2004). The condition $p_1^T E p_0 = 0$ is known as the epipolar constraint and is the same result obtained in the perspective case. This shows that the epipolar constraint is independent of the shape of the image surface.

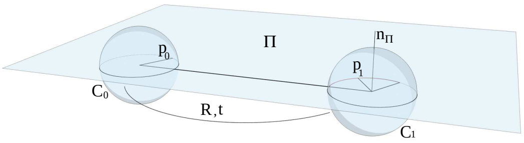

Figure 3: Epipolar geometry for two spherical images.

2.3.2 Pose Estimation

There are mainly two techniques for computing camera poses. The first is useful for *relative* pairwise pose estimation, typically when only 2D image correspondences (2D-2D correspondences) are available. Without loss of generality, one of the cameras is assumed as reference and R and t represent the pose of the second camera. In this case, R and t may be determined with e.g. the 5-point algorithm (Stewénius et al., 2006). The second technique is normally used when a number of 3D scene points and their respective projections onto an image are known, i.e. a set of 2D-3D correspondences is available. This configures a *Perspective-n-point* (PnP) problem, which can be solved with a minimum of 6 correspondences (Quan and Lan, 1999).

3 THE PROPOSED APPROACH

Given a set of images of a scene, our goal is to accurately estimate the pose of all cameras as well as to recover a sparse 3D point cloud of the underlying scene representing its geometry. The set of central projection cameras is then defined as

$$\mathcal{C} = \left\{ C_j = \left[\hat{R}_j | \hat{t}_j \right] \mid \hat{R}_j \in SO(3),\, \hat{t}_j \in \mathbb{R}^3 \right\}, \quad (1)$$

where $j = 0, .., M-1$, M is the total number of cameras and $\hat{R}_j$ and $\hat{t}_j$ are the rotation matrix and translation vector representing the estimated pose of camera C_j. To aid the non-linear optmization, we adopt an axis-angle parameterization for the rotation matrix and C_j is then parameterized by a vector $\rho_j \in \mathbb{R}^6$. All together, the cameras are parameterized by a vector $\rho \in \mathbb{R}^m$, with $m = 6M$.

Likewise, we denote the set of sparse 3D points reconstructed along with the camera poses as

$$\mathcal{P} = \left\{ \hat{P}_i \in \mathbb{R}^3 \right\}, \quad (2)$$

where $i = 0, .., N-1$, N is the number of points and $\hat{P}_i$ holds the estimated coordinates of a scene point P_i.

We then formulate the problem of recovering all cameras' poses along with a sparse point representation of the scene as a non-linear optimization problem. More precisely, the parameter vector ρ is optimized in order to minimize

$$\min_{\rho} \sum_{i=0}^{N-1} \sum_{j=0}^{M-1} f_{ij}(\rho), \quad (3)$$

where $f_{ij}(\rho)$ is a cost function for each point $\hat{P}_i$ and camera C_j. The parameters ρ^+ that minimize Eq. 3 are the sought camera poses. Then, ρ^+ is used to update the points $\hat{P}_i$ to obtain the sparse scene representation.

3.1 Reprojection Error

The reprojection error of a point $\hat{P}_i$ on camera C_j is computed as

$$e_{ij}(\rho) = cos^{-1}(p_{ij}\hat{p}_{ij}), \quad (4)$$

where $p_{ij}\hat{p}_{ij}$ is the scalar product between the expected projection p_{ij} and the measured projection $\hat{p}_{ij}$

obtained with $\hat{P}_i$, $\hat{R}_j$ and $\hat{t}_j$. The expected projection p_{ij} is determined by the keypoint location corresponding to P_i. Note that as $-1 \leq p_{ij}\hat{p}_{ij} \leq 1$, we have $0 \leq e_{ij}(\rho) \leq \pi$ and it is not necessary to take the absolute value in Eq. 4. Furthermore, we do not use any approximation of the reprojection error as in (Pagani and Stricker, 2011). As we aim at high accuracy, the error defined in Eq. 4 is the exact geodesic distance, i.e. the exact angular deviation, between p_{ij} and $\hat{p}_{ij}$. Together, all reprojection errors of a given $\hat{P}_i \in \mathcal{P}$ may be expressed as a vector $e_i(\rho) \in \mathbb{R}^M$. Additionally, to each point P_i we associate a visibility map

$$\mathcal{V}_i = \left\{(C_j, p_{ij}) \mid C_j \in \mathcal{C},\ p_{ij} \in \mathcal{S}^2\right\}, \qquad (5)$$

where $\mathcal{S}^2$ represents the unit sphere. We denote the pair (C_j, p_{ij}) as the *observation* of a scene point P_i on camera C_j. The existence of (C_j, p_{ij}) implies that P_i is visible on camera C_j. Taking the visibility map into account allows to reduce the dimensionality of $e_i(\rho)$ from M to $|\mathcal{V}_i|$, where $|\mathcal{V}_i|$ is the number of observations of P_i. Consequently, the dimensionality of $e_i(\rho)$ is no longer fixed. Instead, it is adapted to the visibility of the corresponding point P_i.

3.2 Minimizing the Reprojection Error

Finding the camera poses and scene structure as described above can be achieved by solving a bundle adjustment problem (Triggs et al., 1999), i.e. by minimizing the reprojection error with respect to all existing 3D points. This allows us to rewrite Eq. 3 in the form shown in Eq. 6. However, different from the classical bundle adjustment, we do not consider the 3D point coordinates as parameters to optmize. Instead, only the camera parameters are used. This leads to two important advantages. First, the dimension of the parameter search space is strongly reduced, simplifying and speeding up non-linear refinement. Second, the set of 3D points used to solve Eq. 6 may be dynamically changed, allowing to use only the best, consistent, points.

$$\min_{\rho} \sum_{i=0}^{N-1}\sum_{j=0}^{M-1} \gamma_{ij} e_{ij}(\rho),\ \gamma_{ij} = \begin{cases} 1,\ if\ C_j \in \mathcal{V}_i \\ 0,\ otherwise \end{cases} \qquad (6)$$

In practice, we use (Agarwal et al., 2010) as the core non-linear solver upon which SPHERA is built. In addition, we solve a modified version of Eq. 6, where only the most reliable points are used. These points are defined as

$$\mathcal{P}^* = \left\{\hat{P}_i \in \mathcal{P} \mid e_{ij}(\rho) < \tau,\ \forall (C_j, \hat{p}_{ij}) \in \mathcal{V}_i\right\}, \qquad (7)$$

where τ is a threshold imposed to all individual reprojection errors $e_{ij}(\rho)$.

4 EVALUATION

4.1 Preliminaries

Keypoints are detected and matched using the method proposed in (Gava et al., 2013), where a multi-scale keypoint detector and matcher was developed for high resolution spherical images. Nonetheless, it is worth mentioning that SPHERA is completely independent of how keypoints are detected, described and matched. Consequently, any other keypoint detector and matcher may be adopted (see Section 4.3).

We validate our framework using synthetic spherical as well as real perspective and spherical images. The resolution of all spherical images presented below is 14142 × 7071 (100 Mega-pixels). Experiments are divided into four categories: The first category consists of a set of synthetic spherical cameras where the goal is to validate our framework on spherical images using groundtruth. The second is composed exclusively of real perspective images. Here, the idea is to show that our framework is suitable for standard SfM, i.e. it may be used even when no spherical image is available. The third category consists of spherical images only, where we compared SPHERA to the work presented in (Pagani and Stricker, 2011) in two different real world scenarios. The fourth and last category is a hybrid dataset, i.e. real perspective and spherical images are used simultaneously. The aim is to demonstrate SPHERA's ability to improve scene geometry estimation whenever more images are available, independent of their types[1]. Whenever available, groundtruth data is used for evaluation. Otherwise, we rely on the global mean reprojection error computed taking all images and all reconstructed points into account.

4.2 Synthetic Dataset

An artificial room with flat walls and dimensions 4x4x3 meters was created using (Blender, 2014) and 9 spherical images were rendered (see Fig. 4-(a)). The poses of these artificially generated cameras were used as groundtruth. Additionally, the depth map shown in Fig. 4-(b) was stored and serves to measure the accuracy of the recovered scene geometry.

After detecting and matching keypoints with Gava's approach, camera poses and scene structure were recovered with SPHERA. Residual errors were computed in the following way. The position error is the Euclidean distance between the groundtruth and estimated camera positions. To measure the orientation error, we chose a function presented in (Huynh,

[1] Assuming central projection cameras.

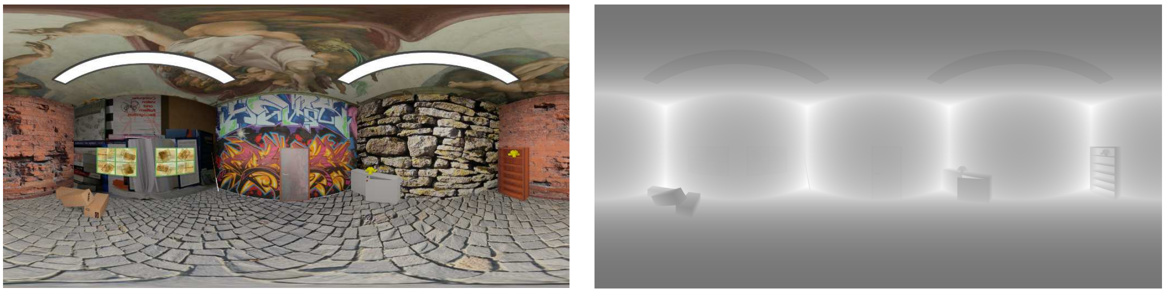

(a) (b)

Figure 4: (a) Sample image of the synthetic dataset. (b) Groundtruth depth map used to evaluate the accuracy of scene geometry estimation (contrast enhanced to improve visualization).

2009) and defined as $\|log\left(R\hat{R}^T\right)\|$, with R the desired rotation and $\hat{R}$ the estimated rotation matrix. This is a metric in $SO(3)$ and can be efficiently computed with quaternions. For details we refer to (Huynh, 2009). Table 1 summarizes the errors in camera pose estimation for . Although very small, these values are not zero mainly due to the precision of detected keypoint locations.

Table 1: Errors in camera pose estimation for the synthetic dataset. Mean and standard deviation are identified by μ and σ, respectively.

	orient. error [degree]	**pos. error** [cm]
μ	6.72×10^{-5}	1.92×10^{-3}
σ	1.73×10^{-4}	3.2×10^{-3}

Here, we also evaluated the influence of the accepted reprojection error τ (see Eq. 7) on the recovered camera poses and scene structure. We repeated the experiment varying τ within the interval $[\tau_{min},\tau_{max}]$. Although τ is an angular deviation, for convenience values are converted and presented in pixels. We chose τ_{min} and τ_{max} to be equivalent to 1 and 5 pixels, respectively.

We noticed that the impact of varying τ on camera pose estimation was neglectable, i.e. the values presented in Table 1 remained constant in practice. This happens due to the fact that, although τ varies by a factor of 5, the global mean reprojection error remains in the interval $[0.365, 0.406]$ pixels (see Fig. 5). However, the same does not hold for the recovered scene structure and deserves attention. We compute the residual error of a reconstructed point $\hat{P}_i$ as $\|\hat{P}_i - P_i\|$, where the coordinates of P_i are obtained as follows. A virtual spherical camera is located at the origin of the global coordinate system. The projection of $\hat{P}_i$ onto this virtual camera delivers $p_i^{'}$. Then $P_i = I_{dm}\left(p_i^{'}\right)p_i^{'}$, where $I_{dm}\left(p_i^{'}\right)$ is the groundtruth depth retrieved from the stored depth map. Not surprisingly, the accuracy of the recovered scene geometry correlates with the mean reprojection error, as depicted in Fig. 5.

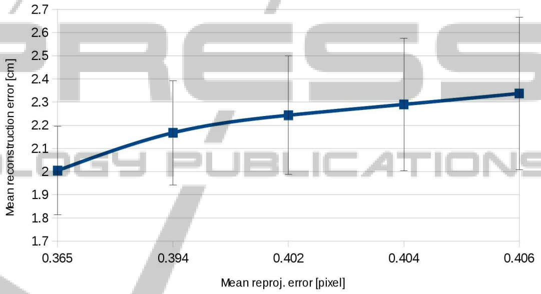

Figure 5: Influence of the mean reprojection error on the accuracy of recovered scene geometry. Vertical bars show the respective standard deviations scaled down by a factor of 10. Values were computed using all reconstructed points (over 30 thousand).

4.3 Perspective Datasets

To validate our approach on perspective images, we compared it to Bundler (Snavely et al., 2006), a popular software developed for SfM on standard perspective images. Bundler is the camera calibration tool currently used in (Furukawa and Ponce, 2008), (Agarwal et al., 2009), (Furukawa et al., 2010) and is publicly available.

The experiments presented in this section were carried out on the datasets published in (Strecha et al., 2008). For each dataset, we ran Bundler on the original images and SPHERA on the corresponding warped images as shown in Fig. 2. To ensure a fair comparison, we ran our pipeline using the same keypoints detected by Bundler (Lowe, 2004) after warping their coordinates to the unit sphere. This eliminates the influence of image feature location on the evaluation. Moreover, it shows SPHERA's independence of keypoint detectors as pointed out in Section 4.1. Results on camera pose estimation are summarized in Fig. 6. Orientation errors were ob-

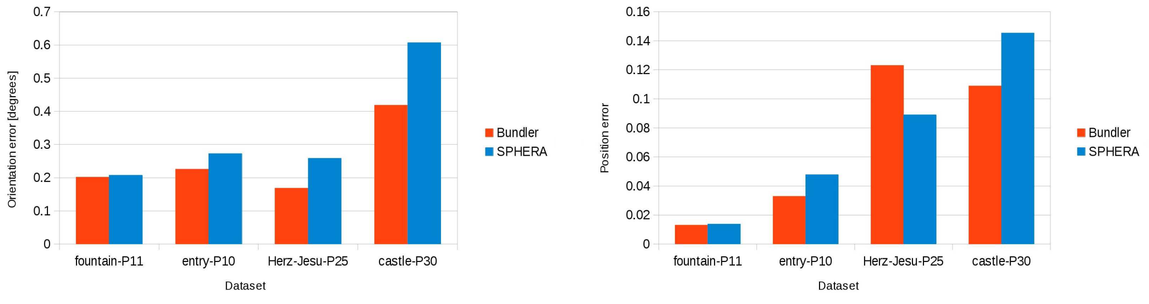

(a) (b)

Figure 6: (a) Orientation error and (b) position error on perspective image datasets obtained with Bundler and SPHERA. See text for details.

tained as in the previous section. Position errors, however, were computed after preprocessing the estimated camera positions. To account for the differences in scale, the baseline between the closest camera pair was normalized and the remaining camera positions were scaled accordingly. After that, the Euclidean distance was measured as in Section 4.2.

As can be seen, Bundler performs slightly better and the reason is as follows. Bundler works exclusively on perspective images and optimizes the camera poses along with their individual intrinsic parameters such as focal length and lens distortion. In contrast, SPHERA has been designed to operate on any kind of central projection camera, but the optimization of intrinsic parameters has not been integrated yet. Therefore, for the experiments presented in this section, we used a constant focal length in our pipeline and a variable focal length for Bundler. In fact, the differences observed in Fig. 6 are proportional to the variance of the focal length within each dataset, see Table 2. The exception is Herz-Jesu-P25, where Bundler delivers smaller orientation error whereas SPHERA provides better camera positions.

Table 2: Variation of focal lengths estimated with Bundler. The second column shows the standard deviation and the third column the difference between maximum and minimum values. Note that, except for the Herz-Jesu-P25 dataset, the differences in Fig. 6 are proportional to the variation of the focal length.

dataset	σ_f [pixel]	**range** [pixel]
fountain-P11	8.49	23.02
entry-P10	10.97	28.41
Herz-Jesu-P25	4.01	16.15
castle-P30	20.44	118.86

4.4 Spherical Datasets

In this section we compare SPHERA and the approach presented in (Pagani and Stricker, 2011). We ran both pipelines on two datasets. The first dataset consists of 9 spherical images captured inside one of the Mogao Caves, in China. The second dataset contains 35 spherical images taken at the Saint Martin Square in Kaiserslautern, Germany, and represents outdoors, more challenging, environments. Due to the lack of groundtruth data for these datasets, we based our evaluation on the global mean reprojection error. The assumption is that the correlation observed in Section 4.2 can be used to infer the relative accuracy of the estimated scene geometry.

As can be seen in Fig. 7, SPHERA improves the reprojection error on both datasets, specially on the St. Martin Square. In the case of the Mogao Cave, due to its simple geometry and rich texture (Fig. 8-(a)), only few points are discarded based on Eq. 7, what explains the small difference in the reprojection error for this dataset. The St. Martin Square dataset is more challenging (Fig. 8-(b)). It contains many low textured regions, depth discontinuites, occlusions as well as repetitive patterns. Therefore, several points are inconsistent and discarding them from the camera pose estimation leads to the difference observed in Fig. 7. These results suggest that SPHERA delivers more accurate scene structures. Figure 8 displays the sparse point clouds yielded by our framework, where details of the surroundings are accurately reconstructed.

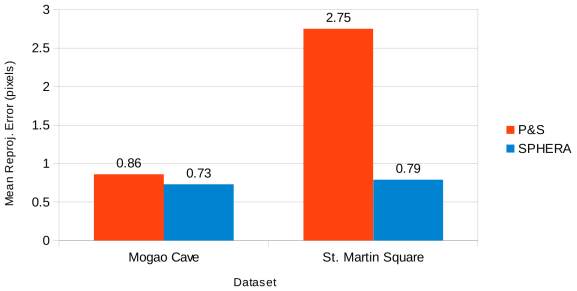

Figure 7: Global mean reprojection error on spherical image datasets obtained with (Pagani and Stricker, 2011) and SPHERA. See text for details.

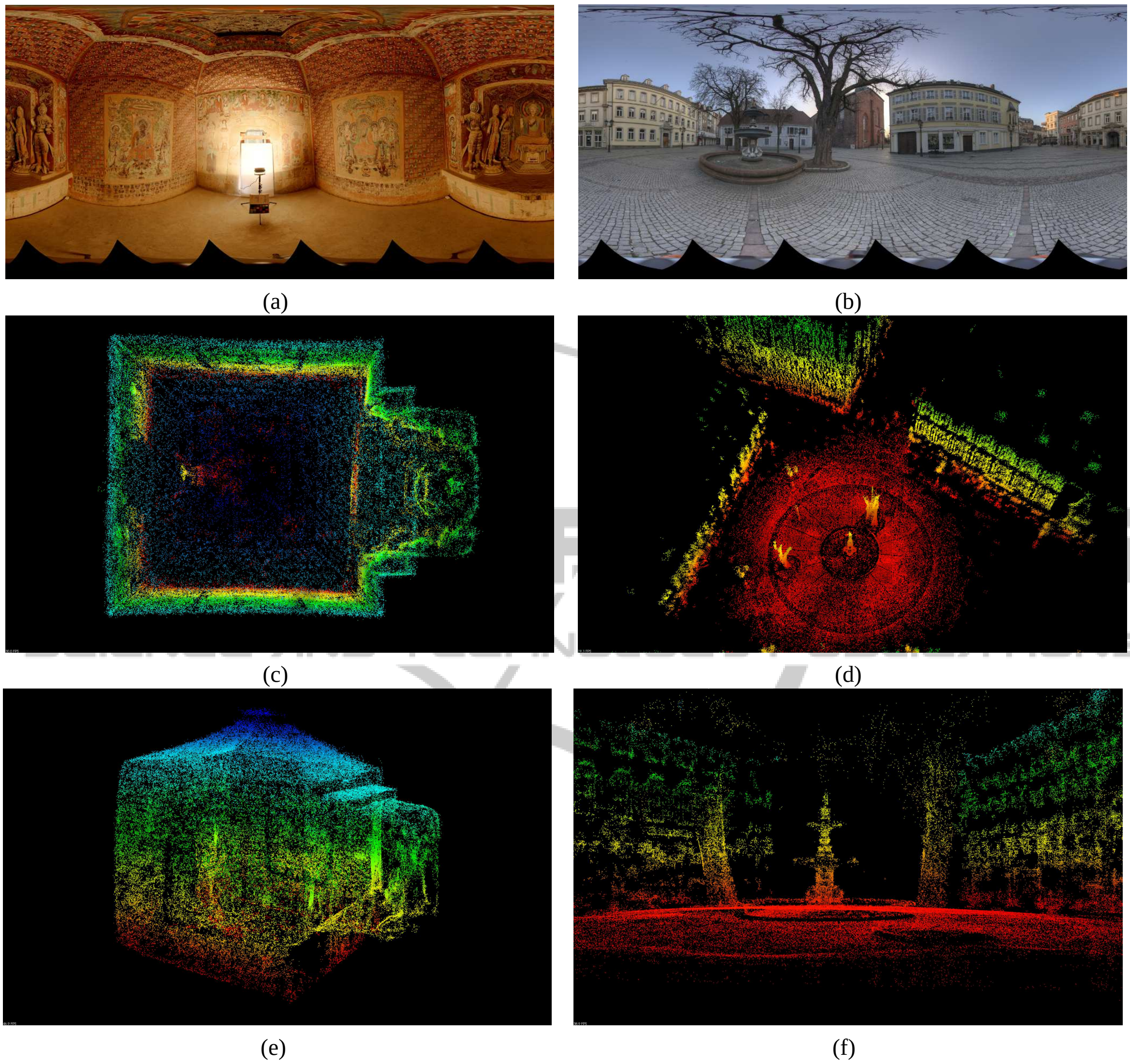

Figure 8: First row: Sample images of the Mogao Cave and St. Martin Square datasets. Second and third rows: reconstructed point clouds delivered by SPHERA, containing approximately 106000 and 197000 3D points for the Mogao Cave and St. Martin Square, respectively.

4.5 Hybrid Dataset

In this section we evaluate the SPHERA framework on a hybrid dataset composed of perspective and spherical images. The idea is to show that our framework naturally handles different central projection cameras simultaneously. This dataset is composed of the same 35 spherical images used in the previous experiment and additional 11 perspective images of resolution 3888×2592 pixels. As shown in Fig. 9, the reprojection error obtained with spherical images (same as previous experiment) is better than the error for perspective images.

The main reason spherical camera pose estimation is better than its perspective counterpart is due to their wide field of view. As can be seen in Fig. 10, matches between spherical images cover the entire scene and thus impose more constraints on cameras' poses. As expected, the reprojection error decreases when perspective and spherical images are used simultaneously.

5 CONCLUSIONS

This paper presents SPHERA, a novel unifying Structure from Motion framework designed for central projection cameras. The goal is to cover the gaps be-

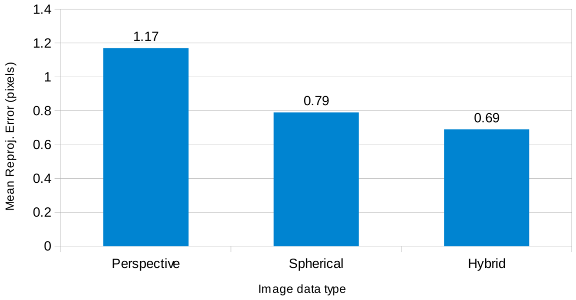

Figure 9: Global mean reprojection error for the hybrid St. Martin Square experiment. Note how it decreases when perspective and spherical images are used together.

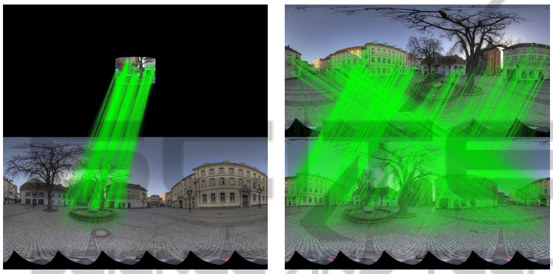

(a) (b)

Figure 10: (a) Symmetric matches between a warped perspective image and a spherical image. Matches are drawn on their corresponding pixel maps to ease visualization. (b) Symmetric matches between two full spherical images.

tween algorithms developed for perspective, spherical and catadioptric images. Through extensive quantitative evaluation on synthetic and real image sequences, we showed that our approach delivers high quality camera pose as well as scene geometry estimations when compared to state of the art approaches optimized for specific camera types.

Future work aims at integrating the optimization of intrinsic parameters to increase the accuracy of perspective cameras pose estimation. Additionally, we plan to validate our framework on larger, hybrid image datasets, supported by groundtruth data. Finally, SPHERA will be the underlying SfM mechanism in our upcoming dense multi-view reconstruction approach.

ACKNOWLEDGEMENTS

This work was funded by the project DENSITY (01IW12001). The authors would like to thank Richard Schulz for the creation of the synthetic dataset.

REFERENCES

Agarwal, S., Mierle, K., and Others (2010). Ceres solver. https://code.google.com/p/ceres-solver/.

Agarwal, S., Snavely, N., Simon, I., Seitz, S. M., and Szeliski, R. (2009). Building rome in a day. In *ICCV*, pages 72–79, Kyoto, Japan.

Aly, M. and Bouguet, J.-Y. (2012). Street view goes indoors: Automatic pose estimation from uncalibrated unordered spherical panoramas. In *WACV*, pages 1–8. IEEE.

Anguelov, D., Dulong, C., Filip, D., Frueh, C., Lafon, S., Lyon, R., Ogale, A., Vincent, L., and Weaver, J. (2010). Google street view: Capturing the world at street level. *Computer*, 43.

Bagnato, L., Frossard, P., and Vandergheynst, P. (2011). A Variational Framework for Structure from Motion in-Omnidirectional Image Sequences. *Journal of Mathematical Imaging and Vision*, 41(3):182–193.

Blender (2014). http://www.blender.org/. Retrieved October 19, 2014.

Chang, P. and Hebert, M. (2000). Omni-directional structure from motion. In *OMNIVIS*, Washington, DC, USA. IEEE Computer Society.

Civetta (2009). http://www.weiss-ag.org/solutions/civetta/. Retrieved October 16, 2014.

Furukawa, Y., Curless, B., Seitz, S. M., and Szeliski, R. (2010). Towards internet-scale multi-view stereo. In *CVPR*.

Furukawa, Y. and Ponce, J. (2008). Accurate, dense, and robust multi-view stereopsis. *IEEE Transactions on Pattern Analysis and Machine Intelligence*, 01(01):1–14.

Gava, C. C., Hengen, J.-M., Taetz, B., and Stricker, D. (2013). Keypoint detection and matching on high resolution spherical images. In *ISVC*, pages 363–372, Rethymnon, Crete, Greece.

Geyer, C. and Daniilidis, K. (2001). Catadioptric projective geometry. *Int. Journal of Computer Vision*, 43:223–243.

Hartley, R. I. and Zisserman, A. (2004). *Multiple View Geometry in Computer Vision*. Cambridge University Press, ISBN: 0521540518, second edition.

Huynh, D. Q. (2009). Metrics for 3d rotations: Comparison and analysis. *Journal of Mathematical Imaging and Vision*, 35(2):155–164.

Kangni, F. and Laganiere, R. (2007). Orientation and pose recovery from spherical panoramas. *ICCV*, 0:1–8.

LizardQ (2014). http://www.lizardq.com. Retrieved October 16, 2014.

Lowe, D. G. (2004). Distinctive image features from scale-invariant keypoints. *Int. Journal of Computer Vision*, 60:91–110.

Ma, Y., Soatto, S., Kosecka, J., and Sastry, S. (2003). *An invitation to 3D vision, from images to models*. Springer Verlag.

Micusik, B. and Pajdla, T. (2006). Structure from motion with wide circular field of view cameras. *IEEE Trans. Pattern Anal. Mach. Intell.*, 28(7):1135–1149.

Pagani, A. and Stricker, D. (2011). Structure from motion using full spherical panoramic cameras. In *OMNIVIS*.

PTgui-Pro (2014). New house internet services b.v. http://www.ptgui.com. Retrieved October 16, 2014.

Quan, L. and Lan, Z. (1999). Linear n-point camera pose determination. *IEEE Trans. Pattern Anal. Mach. Intell.*, 21(8):774–780.

Seitz-Roundshot (2014). http://www.roundshot.ch. Retrieved October 16, 2014.

Snavely, N., Seitz, S. M., and Szeliski, R. (2006). Photo tourism: exploring photo collections in 3D. In *ACM SIGGRAPH 2006 Papers*, SIGGRAPH, pages 835–846, New York, NY, USA. ACM.

Stewénius, H., Engels, C., and Nistér, D. (2006). Recent developments on direct relative orientation. *Journal of Photogrammetry and Remote Sensing*, 60:284–294.

Strecha, C., von Hansen, W., Van Gool, L., Fua, P., and Thoennessen, U. (2008). On Benchmarking Camera Calibration and Multi-View Stereo for High Resolution Imagery. In *Proceedings of the IEEE Conference on Computer Vision and Pattern Recognition*.

Torii, A., Imiya, A., and Ohnishi, N. (2005). Two- and Three- View Geometry for Spherical Cameras. In *OMNIVIS*.

Triggs, B., Mclauchlan, P. F., Hartley, R. I., and Fitzgibbon, A. W. (1999). Bundle adjustment: A modern synthesis. In *Proc. of the International Workshop on Vision Algorithms: Theory and Practice*, pages 298–372.